enough to generate the observed 1-s splitting, unless the anisotropy is >10% which is unrealistic for subcrustal lithosphere. Therefore we conclude that, at least in the vicinity of the rift zone, the source of anisotropy is in the asthenosphere.

The fast direction for the southern part of the profile is roughtly east–west. This may have been generated in a layer of mantle deformed by the collision of India and Asia. It could also be a relict from the ancient past. However, this fast direction is consistent with the dominant direction found across the Tibetan plateau[26]. Both the Tibetan and the Mongolia plateaus have been deformed by Cenozoic deformation related to the collision. The observed fast directions in both regions may have the same origin, that is, the continental collision.

Horizontal upper-mantle flow has previously been inferred using SKS splitting at six stations positioned along the axis of the Rio Grande rift[27] of the western United States. The mean splitting ranges from 0.9 to 1.5 s, with the fast directions being parallel or subparallel to the rift axis. The results were interpreted as being caused by the longitudinal component of a three-dimensional small-scale convection cell associated with the Rio Grande rift. Unfortunately, comparison of this earlier study with our results cannot readily be made as the Baikal rift stations were installed exclusively along a profile across the rift and not along it.

Thus, we suggest that the observed orientation of the anisotropy around Lake Baikal is the result of uppermost-mantle flow associated with recent tectonics. The results in the far south of the study region can be explained by the shear field associated with the collision of India and Asia, whereas those from either side of the Baikal rift reflect the rift's opening. Other studies[4,25] have shown that the asthenosphere upwarps in a broad zone extending either side of Lake Baikal, reaching the base of the crust at the lake itself. The inferred flow responsible for the upwarp is expected to remove ancient anisotropy. As at the mid-Atlantic rift, the fast direction on either side of the Baikal rift is normal to the rift axis. Measurements of vertical anisotropy along the Baikal rift axis will be required to identify whether upwelling mantle flow also occurs directly beneath the rift as is observed on the Mid-Atlantic Ridge[9]. Lithosphere thinning caused by mantle flow would produce a zone of inherent weakness. This can explain how the stresses from the collision of India and Asia could have induced Baikal rifting[12] at such a great distance from the zone of collision. □

Received 20 May; accepted 29 July 1994

1. Parker, E. C., Davis, P. M., Evans, J. R., Iyer, H. M. & Olsen, K. H. *Nature* **312,** 354–356 (1984).
2. Davis, P. M. *Tectonophysics* **197,** 309–325 (1991).
3. Zorin, Yu. A. *Tectonophysics* **73,** 91–104 (1981).
4. Gao, S. *et al. J. geophys. Res.* **99,** 15319–15330 (1994).
5. Babuska, V. & Cara, M. *Seismic Anisotropy in the Earth* (Kluwer, Dordrecht, 1991).
6. Vinnik, L. P., Makeyeva, L. I., Milev, A. & Usenko, A. *Geophys. J. Int.* **111,** 433–447 (1992).
7. Makeyeva, L. I., Vinnik, L. P. & Roecker, S. W. *Nature* **358,** 144–147 (1992).
8. Hess, H. *Nature* **203,** 629–631 (1964).
9. Blackman, D. K., Orcutt, J. A., Forsyth, D. W. & Kendall, J. M. *Nature* **366,** 675–677 (1993).
10. Raitt, R. W., Shor, G. G. Jr, Francis, T. J. G. & Morris, G. B. *J. geophys. Res.* **74,** 3095–3109 (1969).
11. Zonenshain, L. P. & Savostin, L. A. *Tectonophysics* **76,** 1–45 (1981).
12. Molnar, P. & Tapponnier, P. *Science* **189,** 419–426 (1975).
13. Turcotte, D. L. & Emerman, S. H. *Tectonophysics* **94,** 39–51 (1986).
14. Savage, M. K., Silver, P. G. & Meyer, R. P. *Geophys. Res. Lett.* **17,** 21–24 (1990).
15. Vinnik, L. P., Kosarev, G. L. & Makeyeva, L. I. *Proc. Acad. Sci. U.S.S.R.* **278,** 1335–1339 (1984).
16. Kind, R., Kosarev, G. L., Makeyeva, L. I. & Vinnik, L. P. *Nature* **318,** 358–361 (1985).
17. Silver, P. G. & Chan, W. W. *Nature* **335,** 34–39 (1988).
18. Ansel, V. & Nataf, H. C. *Geophys. Res. Lett.* **16,** 409–412 (1989).
19. Vinnik, L. P., Farra, V. & Romanowicz, B. *Bull. seism. Soc. Am.* **79,** 1542–1558 (1989).
20. Makeyeva, L. I., Plesinger, A. & Horalek, J. *Phys. Earth planet. Inter.* **62,** 298–306 (1990).
21. Silver, P. G. & Chan, W. W. *J. geophys. Res.* **96,** 16429–16454 (1991).
22. Zoback, M. L. *J. geophys. Res.* **97,** 11703–11728 (1992).
23. McNamara, D. E. & Owens, T. J. *J. geophys. Res.* **98,** 12003–12017 (1993).
24. Sheriff, R. E. & Geldart, L. P. *Exploration Seismology* (Cambridge Univ. Press, 1982).
25. Zorin, Yu.A., Yu.A., Kozhevnikov, V. M., Novoselova, M. R. & Turutanov, E. K. *Tectonophysics* **168,** 327–337 (1989).
26. McNamara, D. E., Owens, T. J. & Silver, P. G. *J. geophys. Res.* **99,** 13655–13666 (1994).
27. Sandovol, E., Ni, J., Ozalaybey, S. & Schlue, J. *Geophys. Res. Lett.* **19,** 2337–2340 (1992).
28. Chastel, Y. B., Dawson, P. R., Wenk, H.-R. & Bennett, K. *J. geophys. Res.* **98,** 17757–17771 (1993).

ACKNOWLEDGEMENTS. We thank N. A. Logatchev for his support of this joint preject, and R. Girdler for comments and discussions. We also thank P. Molnar and R. Keller for critical reviews of the manuscript. The REFTEK recorders and some of the seismometers were provided by the PASSCAL Instrument Center at Lamont-Doherty Earth Observatory. Field work in Russia was supported by the Russian Academy of Sciences; work at UCLA and the University of Wisconsin were supported by DARPA.

Multiple processing streams in occipitotemporal visual cortex

Edgar A. DeYoe*, Daniel J. Felleman†‡, David C. Van Essen‡§ & Evelyn McClendon†

* Department of Cellular Biology and Anatomy, The Medical College of Wisconsin, 8701 Watertown Plank Road, Milwaukee, Wisconsin 53226, USA
† Department of Neurobiology and Anatomy, University of Texas Medical School, Houston, Texas 77030, USA
‡ Division of Biology 216–76, California Institute of Technology, Pasadena, California 91125, USA

THE earliest stages of cortical visual processing in areas V1 and V2 of the macaque monkey contain internal subdivisions ('blobs' and 'interblobs' in layer 4B in V1; thin, thick and interstripes in V2) that are selectively interconnected and contain neurons with distinctive visual response properties[1–10]. Here we use anatomical pathway tracing to demonstrate that higher visual areas, V4 and the ventral posterior inferotemporal cortex, each contain anatomical subdivisions that have distinct input and output projections. These findings, in conjunction with others[11–15], suggest that modularity and multistream processing within individual cortical areas are widespread features of neocortical organization.

§ Present address: Department of Anatomy and Neurobiology, Washington University School of Medicine, St Louis, Missouri 63110, USA.

We injected two retrograde tracers (three tracers in one case) into nearby sites in V4 of five hemispheres from three macaque monkeys. For three pairs of injections, strongly segregated clusters of cells labelled by each tracer were found within extrastriate visual areas V2, V3/V3A, V4v/VP and PITv (see legend to Table 1 for abbreviations). Figure 1 illustrates results from one such case (case 1 in Table 1) in which bisbenzimide and nuclear yellow were injected at sites 4.3 mm apart in V4 (Fig. 1*a*). Each injection labelled several bands of cells throughout a 14-mm swath of dorsal V2 (Fig. 1*b*), demonstrating that the two injections involved similar parts of the perifoveal visual field representation. The bisbenzimide was concentrated in the pale-staining interstripes revealed by cytochrome oxidase histochemistry, whereas the nuclear yellow was centred along a subset of the dark cytochrome-oxidase-staining stripes (red outlines in Fig. 1*b*). We infer that the nuclear yellow was primarily in the thin-stripe compartments (even in regions where the pattern was somewhat irregular), because it has been shown elsewhere that (1) the thick stripes do not have a substantial projection to V4 (refs 1, 3, 12, 14) and (2) anatomical segregation is maintained even within regions of irregular stripe geometry[3,14].

The pattern of retrograde labelling in the remainder of extrastriate cortex is shown as a three-dimensional reconstruction of occipitotemporal cortex in Fig. 1*a*, as a single section through the prelunate gyrus in Fig. 1*c*, and as a two-dimensional map of 'unfolded' cortex in Fig. 1*d*. Throughout occipitotemporal cortex, labelled cells were found in clusters of variable shape and size ranging from ~4 mm^2 to >70 mm^2.

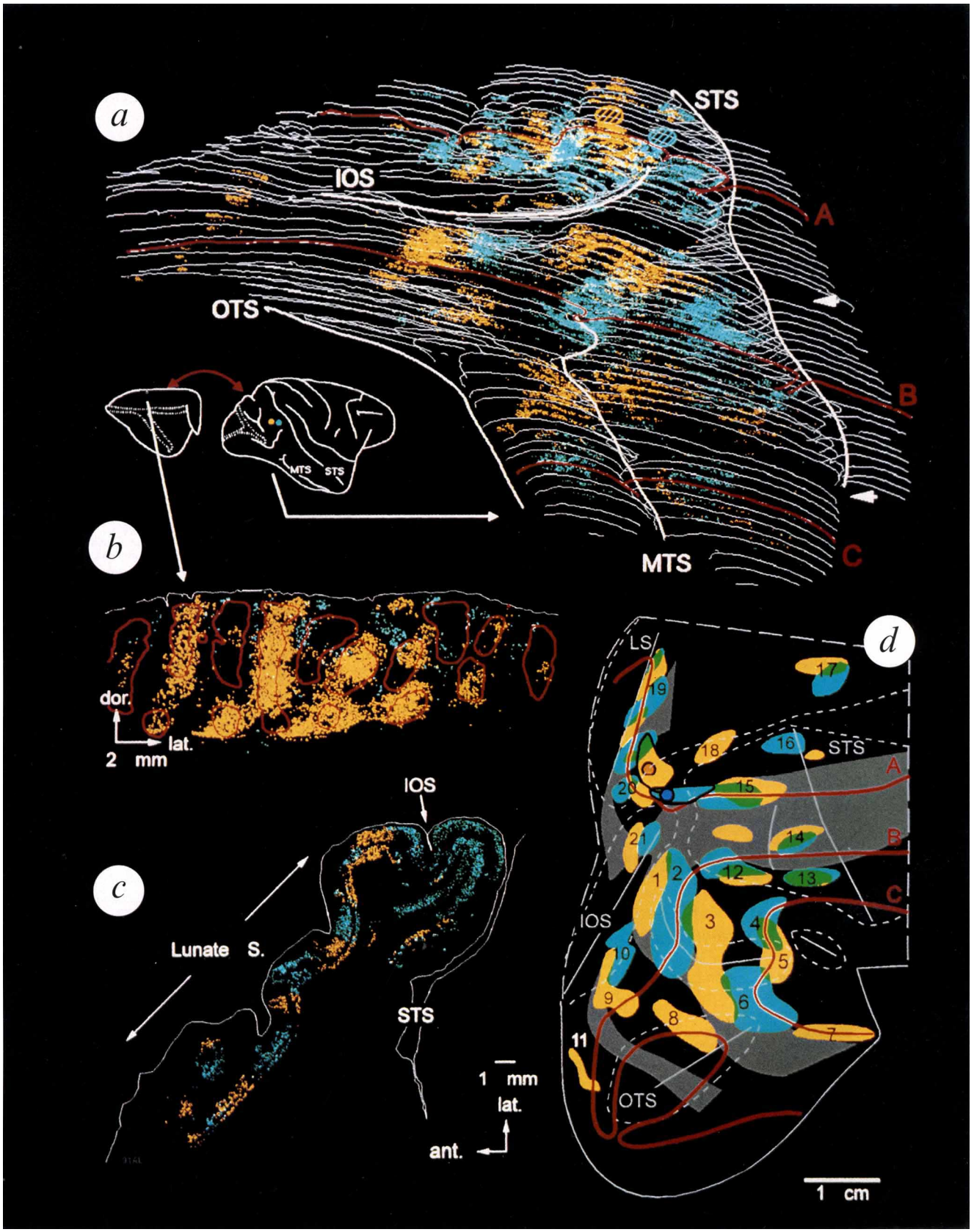

FIG. 1 Segregated, retrograde labelling of extrastriate visual areas following dual tracer injections in V4: *a*, Three-dimensional computer reconstruction of tracer labelling in occipitotemporal cortex visible from the exposed lateral surface of the brain. A Silicon Graphics IRIS workstation with custom software was used for data acquisition and visualization. Crosshatch ovals: approximate core of tracer injection sites. All dense core injection sites in this and other experiments were restricted to cortical grey matter and were within the boundaries of the desired target area as described in ref. 16. Yellow site, 100 nl 3% nuclear yellow (Sigma) in distilled water; blue site, 100 nl 10% bisbenzimide (Sigma) in distilled water. Yellow and blue dots, cells labelled with the respective tracer (occasional white dots are photographic artefacts due to yellow and blue superposition). Thin white and red contours (A, B, C) outline horizontally sliced histological sections (minimum

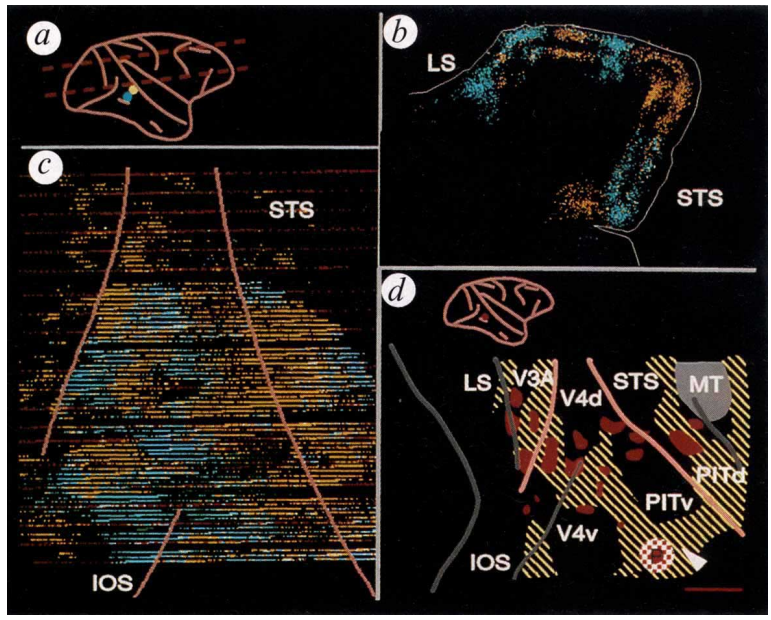

FIG. 2 Clustering of retrograde and anterograde labelling in V4 following tracer injection in posterior inferotemporal cortex (PIT). *a*, Approximate location of tracer injection sites in PIT and range of sections shown in *c* (dashed lines). Blue dot, 250 nl injection of Fast blue (FB); white dot, 250 nl diamidino yellow (DY) placed 5 mm more dorsal at the crown of the STS encroaching on area PITd. *b*, Computer reconstruction of labelling in three superimposed horizontal brain sections through V4 near dorsal tip of inferior occipital sulcus. *c*, Computer reconstruction of retrogradely labelled cells in 80 horizontal brain sections spanning 20 mm dorsoventrally across V4. The three-dimensional stack of sections is shown in a lateral view with the lunate, superior temporal and inferior occipital sulci outlined for reference. Major contours (red lines) are drawn at 1-mm intervals (straight horizontal gaps are due to missing sections). *d*, Anterograde labelling in a different case in which 25 μCi (200 nl) ^{3}H-proline was injected in PITv just above the posterior middle temporal sulcus (red dot on inset view). Clusters of anterogradely labelled terminals in V4 and V3A are marked by multiple red patches on an unfolded, two-dimensional cortical map. Also shown is the distribution of HRP-labelled, callosal-projecting cells (diagonal hatch) used to help identify areal boundaries[14,30]. A, B and C: case 90DR; D, case 90CL.

In many instances, multiple patches could be assigned to individual visual areas using the pattern of interhemispheric connections (grey bands in Fig. 1*d*) as an independent guide to areal boundaries. For example, in inferotemporal cortex there were three large, alternating yellow and blue clusters (numbered 1–3 in Fig. 1*d*) which could be assigned to area PITv by virtue of their proximity to a band of callosal-projecting cells that runs along its posterior boundary[14]. Further anterior in the temporal lobe (to the right in Fig. 1*d*), area CITv also contained multiple clusters. Similarly, the anterior bank of the lunate sulcus including parts of visual areas V3, V3A and V4[16] contained at least 10 distinct, alternating yellow and blue clusters (Fig. 1*c*, *d*). In contrast, labelled clusters within the superior temporal sulcus, especially anteriorly, were more intermixed, as indicated by the green zones of overlap in Fig. 1*d*.

To quantify the degree of segregation, we computed a segregation index designed to yield values near zero in regions of extensive intermixing and values approaching (or occasionally exceeding) unity in regions where segregation was pronounced. Results for all V4 injections are shown in Table 1 (see legend for details of index calculation). Bold-face entries indicate regions that had segregation indices above 0.60 and that also were judged prior to quantitative analysis to have strongly segregated labelling.

In cases 1–3, strong segregation occurred in V2 and in occipitotemporal areas V3A/V3, V4v/VOT and PITv. In contrast, cases 4 and 5A resulted in consistently greater intermixing of the two tracers in V2 and in the aforementioned occipitotemporal regions. Finally, case 5B provided a valuable control condition, because the placement of injections in V4 led to separate regions of label in dorsal V2 that were the most retinotopically segregated of any case, but were predominantly within the same compartments (interstripes). This resulted in strongly intermixed labelling in occipitotemporal cortex, indicating that the degree of segregation correlated better with the compartmental distribution than with the retinotopic segregation of label in V2.

These findings suggest that some extrastriate visual areas project to V4 via at least two populations of output neurons. The projections from each population must terminate in largely segregated patches within V4, because appropriately placed injections labelled one or the other population with little intermixing. Moreover, as the degree of segregation was correlated across V2, V3A/V3 and PITv, the terminal patches derived from each area's projections must be largely coincident in V4.

To determine whether projection neurons inside V4 are also clustered in segregated domains similar to those of afferent terminals, retrograde tracer injections were made into two major targets of V4 projections, areas PITv and PITd. Figure 2*a* shows the location of one pair of injections placed 5 mm apart in PITv (the superior injection may also encroach on PITd). Alternating clusters of cells labelled by each tracer occupied a wide expanse of V4 within the lunate sulcus, prelunate gyrus, and superior temporal sulcus, where the labelling also included area V4t (Fig. 2*b*). An *en face* view of the prelunate gyrus illustrated in Fig. 2*c* shows the overall pattern of clustering in this case. A similar, highly segregated, yet interdigitating pattern of V4 labelling was also observed in two additional cases of dual PITv injections. In these cases, the number and size of labelled clusters ranged from three relatively large patches in one monkey to 8–10 smaller patches in another. In contrast, two more cases of paired PITv injections resulted in complex patterns of labelling in V4 which were partially segregated in some regions and partially inter-

spacing, 0.4 mm). White arrowheads, missing sections at block boundaries. *a* (inset), Removal of occipital cortex permits flattening of V2, exposes anterior bank of lunate sulcus. *b*, View *en face* of tracer labelling in 9 superimposed sections of dorsal V2 spanning 1.0-mm depth. Red outlines represent composite of cytochrome-oxidase-dense regions from 3 additional sections. *c*, Details of tracer labelling in horizontal section marked by red outline 'A' in *a*. Note alternating clusters along bank of lunate sulcus, including portions of V3, V3A and V4d (ref. 16). *d*, Summary map of a manually unfolded cortical map[28] encompassing most of the extrastriate cortex (except V2). Grey areas show concentrations of callosal projecting cells labelled with horseradish peroxidase (Sigma type VI) applied to transsected corpus callosum (some portions are occluded by overlying tracer pattern). Thin dotted lines mark cortex within sulci. Red lines mark unfolded contours of sections partially outlined in red in *a*. Yellow and blue areas indicate labelling by single tracer; green areas indicate mixing. Estimated relationships of labelled patches to visual areas: 1, 2, 3: PITv; 4, 5, 6: CITv; 7: probable TF/TH; 8: VOT; 9, 10: V4v, VP; 11: V2v; 12: PITd; 13: CITd; 14: FST; 15: V4t/MT; 16: probable MST; 17: LIP; 18: probable DP; 19: V3/V3a; 20, 21: V4. Area assignments and nomenclature are from cortical maps in refs 14, 16, 29. IOS, inferior occipital sulcus; MTS, middle temporal sulcus; OTS, occipitotemporal sulcus; STS, superior temporal sulcus (case 91AL).

TABLE 1 Segregation indices for extrastriate visual areas following paired tracer injections in V4

Case	Sep.	V2	V3A/V3	V4v/VOT	PITv	CITv	STS
1	4.3	**0.90**	**0.87**	**0.86**	**0.89**	**0.66**	0.44
2	4.5	**0.92**	C	**0.86**	**0.75**	0.38	0.55
3	4.0	**0.93**	**0.86**	**0.61**	**0.84**	0.37	0.52
4	4.4	0.28	0.35	0.56	0.33	0.12	0.30
5A	2.0	0.46	—	C	0.07	—	0.56
5B	4.0	0.67*	—	C	0.28	—	0.47

The segregation index for each region was calculated in several steps. First, clusters were identified on computerized reconstructions of individual histological sections (Fig. 1c for example) by initially displaying only one tracer label. Each group of cells that was clearly separated from other groups was circumscribed by a rectangular, radially aligned counting window. Groups that were not clearly separated were included in the same counting window. Next, the second tracer labelling was displayed with the first. Any cells that did not fall within the previously established counting windows were circumscribed by additional non-overlapping windows until virtually all cells were included. For each window, cells labelled by the two tracers (denoted as A_i and B_i) were then counted and a distribution index was calculated as $D_i=(A_i-B_i)/(A_i+B_i)$. This index equals zero when the cell number A_i and B_i are equal and approaches ±1 as one or the other label predominates. Next, an overall distribution index for each visual area was calculated as $D_{tot}=(A_{tot}-B_{tot})/(A_{tot}+B_{tot})$, where A_{tot} and B_{tot} were the total number of cells labelled by each tracer within the specified visual area. D_{tot} represents the distribution index that would occur if all labelled cells in the area were uniformly mixed, and it takes into account the different numbers of cells labelled by each tracer. Departures from D_{tot} indicate distributions that were more segregated than expected. Consequently, the index of segregation for each counting window (S_i) was computed as the deviation from D_{tot}: $S_i=|(D_i-D_{tot})|$. Although values of S_i can exceed 1.0 (if D_{tot} is negative), they correctly represent deviations from the uniformly mixed distribution. Final entries in the table are mean of all segregation indices (one for each counting window) calculated for each region. Bold type indicates regions with mean segregation index >0.6 that were judged to be strongly segregated by visual inspection before quantitative analysis. C, clustered labelling, but only one tracer present. Sep, injection site separation (mm). V3A/V3, anterior bank of lunate sulcus containing area V3A and part of V3; V4v/VOT, ventral V4 plus ventral occipital temporal area and ventral posterior area if labelled; PITv, ventral division of posterior inferotemporal cortex; CITv, ventral division of central inferotemporal cortex, also including areas TF and TH when labelled; STS, superior temporal sulcus including areas MT, MST, FST and PITd. Labelling in CITd and AITd was weak but intermixed in case 1 and was too weak for classification in other cases. Case identification: 1:91AL; 2:90LR; 3:85EL; 4:91AR; 5A:90LL; 5B:90LL. * Case 5B in V2 reflects retinotopically based segregation (see text). The tracer bisbenzimide (Sigma) was paired with nuclear yellow (Sigma) in cases 1, 3, 4 and 5B; or with rhodamine-labelled dextrans (Molecular Probes) in cases 2 and 5A.

mixed in others. Finally, two cases of single tracer injections, one in PITv and one in PITd, resulted in V4 labelling which was partially clustered in some regions and more continuous in others.

These results show that V4 contains at least two populations of output neurons that are segregated into clusters of variable extent. Projections to PIT from each population must terminate in largely non-overlapping patches, because some paired injections labelled each population separately. Together with our previous results, this suggests that PITv itself contains anatomically heterogeneous domains.

To study the termination patterns of feedback projections from inferotemporal cortex to V4, we injected anterograde tracers into PITv. Figure 2*d* shows results from a ^{3}H-proline injection that produced a patchy distribution of terminal labelling throughout foveal V4 and adjoining regions. In two other cases, injections of wheat-germ agglutinin–horseradish peroxidase (a dual anterograde/retrograde tracer) into PITv labelled clusters of axon terminals that were often, though not always, in register with clusters of projection neurons within V4. This indicates that in V4, as in V2[15,17,18], the distributions of efferent cell clusters and afferent terminal clusters are correlated but not identical.

The segregated connectivity patterns demonstrated here in occipitotemporal cortex represent an elaboration of two major processing streams which originate in the blob and interblob compartments of V1 and project to V4 via the thin- and interstripe compartments of V2[2,8,19–21]. Presumably the functional characteristics of different modules in V4 and subsequently in PITv are strongly influenced by these inputs, but will be modified by additional cortical and subcortical inputs[16,22] and by cross-connections between streams[2,4,5,16,23–26]. The distinctions between streams may reflect a dichotomy between form and colour perception[6], or alternatively between analyses of object boundaries versus interior surface characteristics[21,27]. Regardless of their specific functions, multiple processing streams are characteristic of individual visual areas at four successive stages of the cortical hierarchy, presumably providing greater flexibility and dynamic control of the multiple types of analysis performed within each area. □

Received 6 April; accepted 20 July 1994.

1. DeYoe, E. A. & Van Essen, D. C. *Nature* **317,** 58–61 (1985).
2. DeYoe, E. A. & Van Essen, D. C. *Trends Neurosci.* **11,** 219–226 (1988).
3. DeYoe, E. A., Hockfield, S., Garren, H. & Van Essen, D. C. *Vis. Neurosci.* **5,** 67–81 (1990).
4. Hubel, D. H. & Livingstone, M. S. *J. Neurosci.* **7,** 3378–3415 (1987).
5. Livingstone, M. S. & Hubel, D. H. *J. Neurosci.* **4,** 309–356 (1984).
6. Livingstone, M. & Hubel, D. *Science* **240,** 740–749 (1988).
7. Maunsell, J. H. R. & Newsome, W. T. *A. Rev. Neurosci.* **10,** 353–401 (1987)
8. Shipp, S. & Zeki, S. *Nature* **315,** 322–324 (1985).
9. Tootell, R. B. H. & Hamilton, S. *J. Neurosci.* **9,** 2620–2644 (1989).
10. Ts'o, D. Y. & Gilbert, C. D. *J. Neurosci.* **8,** 1712–1727 (1988).
11. Born, R. T. & Tootell, R. B. *Nature* **357,** 497–499 (1992).
12. DeYoe, E. A., Felleman, D. J., Knierim, J. J., Olavarria, J. & Van Essen, D. C. *Invest. Ophthal. vis. Sci.* (suppl.) **29,** 115 (1988).
13. Goldman-Rakic, P. S. & Schwartz, M. L. *Science* **216,** 755–757 (1982).
14. Van Essen, D. C., Felleman, D. J., DeYoe, E. A., Olavarria, J. & Knierim, J. *Cold. Spring Harb. Symp. quant. Biol.* **LV,** 679–696 (1990)
15. Zeki, S. & Shipp, S. *Eur. J. Neurosci.* **1,** 494–506 (1989).
16. Felleman, D. J. & Van Essen, D. C. *Cerebral Cortex* **1,** 1–148 (1991).
17. Shipp, S. & Zeki, S. *Eur. J. Neurosci.* **1,** 333–354 (1989).
18. Krubitzer, L. A. & Kaas, J. H. *Brain Res.* **478,** 161–165 (1989).
19. Livingstone, M. S. & Hubel, D. H. *J. Neurosci.* **4,** 2830–2835 (1984).
20. Desimone, R. & Ungerleider, L. G. in *Handbook of Neuropsychology* (eds Boller, F. & Grafman, J.) 267–299 (Elsevier, Amsterdam, 1989).
21. Van Essen, D. C. & DeYoe, E. A. in *The Cognitive Neurosciences* (ed. Gazzaniga, M. S.) 383–400 (MIT Press, Cambridge, MA, 1994).
22. Tanaka, M., Lindsley, E., Lausmann, S. & Creutzfeldt, O. D. *Anat. Embryol.* **181,** 19–30 (1990).
23. Lund, J. S. *A. Rev. Neurosci.* **11,** 253–288 (1988).
24. Malpeli, J. G., Schiller, P. H. & Colby, C. L. *J. Neurophys.* **46,** 1102–1118 (1981).
25. Ferrera, V. P., Nealey, T. A. & Maunsell, J. H. *Nature* **358,** 756–761 (1992).
26. Maunsell, J. H. *Curr. Opin. Neurobiol.* **2,** 506–510 (1992).
27. Grossberg, S. *Percept. Psychophys.* **41,** 87–116 (1987).
28. Van Essen, D. C. & Maunsell, J. H. R. *J. comp. Neurol.* **191,** 255–281 (1980).
29. Ungerleider, L. G. & Desimone, R. *J. comp. Neurol.* **248,** 190–222 (1986).
30. Van Essen, D. C., Newsome, W. T. & Bixby, J. L. *J. Neurosci.* **2,** 265–183 (1982).

ACKNOWLEDGEMENTS. We thank K. Hasselblatt. L. Sisola, E. Earle and J. Weiser for technical assistance, D. Bilitch for developing three-dimensional reconstruction software, and G. Carman and S. Glickerman for assistance with analysis software. This work was supported by separate grants from the National Eye Institute of the US Public Health Service to E.A.D., D.C.V.E. and D.J.F.